

Stress Corrosion Cracking Study of Aluminum Alloys using Electrochemical Noise Analysis

R. C. Rathod¹, S. G. Sapate¹, R. Raman²

¹*Department of Metallurgical and Materials Engineering,
Visvesvaraya National Institute of Technology, Nagpur - 440 010, India.*

²*Department of Metallurgical Engineering and Materials science,
Indian Institute of Technology Bombay, Mumbai-400 076, India.*

Abstract

Electrochemical noise (ECN) analysis of potential and current time series is becoming increasingly popular in corrosion research. There is need to generate the data on corrosion resistance of high strength aluminium alloys, which can be directly useful in material selection and design of alloys. Aluminium alloys mainly AA8090, AA2219 and AA5456 in heat-treated and non heat-treated condition were studied for Stress Corrosion Cracking (SCC) at different amount of loading. Corrosion potential (E_{cor}) vs. time data was obtained for stressed specimen by immersing them for different duration of time in 3.5% NaCl solution at room temperature. The obtained noise data was subjected to conventional and non-linear rescaled range (R/S) analysis to obtain the Hurst exponent. Higher values of Hurst exponent were obtained whenever the material and environment combination led to localized attack by stress corrosion cracking. This has been confirmed in the case of peak aged and solution treated aluminium alloys.

Keywords: Electrochemical noise analysis, Aluminium alloys, Stress corrosion cracking, Hurst exponent.

Corresponding author. Tel: +91-712-2801104; Fax: +91-712-2223230

E-mail address: rcrathod@mme.vnit.ac.in.

Introduction

Aluminum alloys are widely used for aerospace application due to their high specific strength. Localized corrosion of aluminium alloys, which usually appears as pitting, crevice corrosion and in certain cases as stress corrosion cracking. Though aluminium alloys are highly stable in many environments, their use is limited by their susceptibility to localized corrosion such as stress corrosion cracking (SCC) and pitting. Stress corrosion cracking is a complex synergistic interaction of corrosive environments and sustained tensile stress at the exposed surface of metal. In high strength aluminium alloys, SCC is known to occur under ordinary and aqueous environments. The exact mechanism responsible for SCC of susceptible aluminium alloy in a particular corrosion environment remains controversial. However proposed mechanisms are variations of two basic theories; crack propagation by anodic dissolution or by hydrogen embrittlement. It is possible that hydrogen may contribute to SCC of certain tempers of aluminium alloys, although a detailed mechanistic understanding of SCC in aluminium alloys still requires more research [1–5].

The choice of conventional electrochemical techniques depends upon the type of corrosion being investigated. The conventional electrochemical techniques have one common deficiency which involves external electrical perturbation (anodic/cathodic polarization) to some degree, leading to significant departures from the freely corroding techniques. This has led to search for new technique, which is non perturbative (free corroding system) [6, 7]. Ever since the pioneering work by Iverson [8] on the apparently random fluctuations in the open circuit potential of metals and alloys immersed in chloride solutions, there has been a sustained interest leading to exponential growth in publication on corrosion studies using electrochemical noise analysis technique. Electrochemical noise is a well known phenomenon applied to corrosion process characterization in laboratory and industrial practice [8–12]. Hurst exponent (H) has broad applicability to all time series analysis because it is remarkably robust. It can distinguish a random series from nonrandom series, even if the random series is non-Gaussian. Hurst found that most natural systems do not follow a random walk or Gaussian. Hurst formulated a dimensionless ratio by dividing the range by standardization of the observations. Hence the analogies are known as rescaled range analysis(R/S) [13–15].

Uruchurtu and Dawson [16] studied the noise analysis of pure aluminium in 3% sodium chloride solution. It was revealed that the over all noise level tends to decrease with time. The noise analysis suggests that dynamic crack healing process was occurring at defects sites in the pure aluminium oxide film. They also observed that chloride ions, rather than promoting breakdown, were largely responsible for preventing repassivation. Laban et al. [17] advocated electrochemical noise as a possible method for detecting stress corrosion cracking of thin metal sheets in neutral NaCl solution. They concluded that higher rate of corrosion localization occurs in the presence of stress. Loto and Cottis [18] used electrochemical noise measurement technique to monitor the stress corrosion cracking processes of high-strength aluminium alloys and observed intergranular cracking, which was attributed to not only to pits but also to micro cracks developed on the specimen surface during stressing. Gonzalez-Nunez et al. [19] obtained Hurst exponent which demonstrated electrochemical noise time series fractals. It provided a tool for the interpretation of the structure of electrochemical noise data as well as a quantitative measurement of coating performance and corrosion mechanisms.

Liu et al. [20] investigated the influence of applied stresses on the potential noises for 7075– T76 aluminium alloy in 3.5% NaCl solution by various methods such as statistical method, Fourier transform and Wavelet transform. With increase in the applied stresses the mean potential shifted more negatively and the applied stresses also promoted the initiation and propagation of pitting corrosion. Anita and coworkers [21] studied stress corrosion cracking of type 316 stainless steel under unstressed and stressed condition in deareated sodium chloride solution at room temperature using electrochemical noise method. The importance of potential and current records during SCC test was highlighted in their study. In a recent study performed by Na et al. [22] using stochastic theory and shot noise theory, the pitting corrosion was distinguished from uniform corrosion by the frequency of events in the stochastic analysis.

Several studies have proved that the electrochemical noise (ECN) technique is well suited to the detection of localized corrosion processes, which can occur on metal surfaces. Although this technique has been adopted as a satisfactory method for the detection of uniform, pitting and crevice corrosion, but its use for the analysis of complex SCC process is still relatively rare. Therefore the present study was undertaken, to study stress corrosion cracking of different aluminium alloys using electrochemical noise method with constant applied load under fully immersed condition. The specimens of AA2219, AA5456 and

AA8090 of alloys were stressed to obtain E_{corr} Vs time noise data at different time. The essential non-linear time series noise data obtained was subjected to the robust R/S analysis which yielded Hurst exponent. The variations in Hurst exponent from time of immersion to time of fracture were also recorded.

Experimental

Materials

The materials used in the present investigation were AA2219, AA5456 and AA8090 aluminium alloys. The chemical composition and mechanical properties of aluminium alloys are given in table 1 and table 2 respectively. The specimens were prepared in peak aged and solution annealed condition in case of aluminium alloys AA2219 and AA8090 whereas alloy AA5456 was in strain hardened and solution annealed condition.

Table 1 Chemical composition of aluminium alloys (Weight %)

Alloy	Cu	Mg	Si	Fe	Mn	Zn	Li	Ti	Zr	Al
AA2219	6.50	0.008	0.084	0.096	0.29	0.024	–	0.060	–	balance
AA8090	1.8	1.0	0.08	0.1	–	–	2.0	–	0.8	balance
AA5456	–	5.50	0.20	–	0.54	–	–	–	–	balance

Table 2 Mechanical properties of aluminium alloys

Alloy	Tensile strength (MPa)	Yield strength (MPa)	Elongation (%)	Hardness (HB)

AA2219	170–480	70–390	10–18	Up to 130
AA8090	280–560	100–400	10–15	Up to 140
AA5456	300–350	160–260	10–24	Up to 90

Optical microscopy

The specimens with dimensions of 10 x 10 x 2 mm were used for metallographic. The specimens were mounted using cold cure acrylic compound and polished using 1/0, 2/0, 3/0 and 4/0 grades of emery paper, followed by polishing with ½ micrometer diamond paste. The specimens were then cleaned, dried and etched with Keller's reagent and observed under optical microscope.

Stress corrosion testing using electrochemical noise test

Stress corrosion cracking testing on tensile specimens of the AA 2219, AA5456 and AA 8090, as shown in figure 1, were performed using experimental set-up as shown in figure 2 [23].

A spring loaded tensometer was used. The load was applied by compressing the spring. The spring was calibrated before the stress corrosion testing and the spring constant was calculated using the following expression [24].

$$K = Gd^4 / 8D^3n$$

Where, K = spring rate or constant, N/mm

G = modulus of rigidity = 0.85×10^5 N/mm²

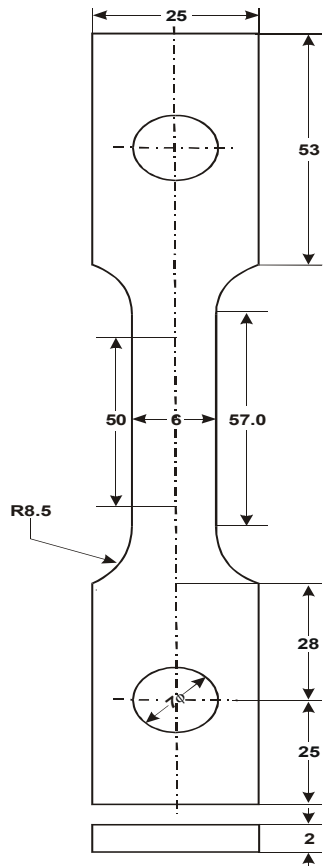
n = number of active coils

d = diameter of steel wire, mm

D = diameter of active coil, mm

In the present investigation spring diameter; d was 24 mm and diameter of active coil; D was 80 mm and number of coils; n were 12. The load to be applied was calculated using the following expression; F = K x X; where F is load in Kilo Newton (KN), K is spring constant = 0.276 KN/mm and X is displacement in mm.

Figure 1: Tensile specimen.



All dimensions are in mm.

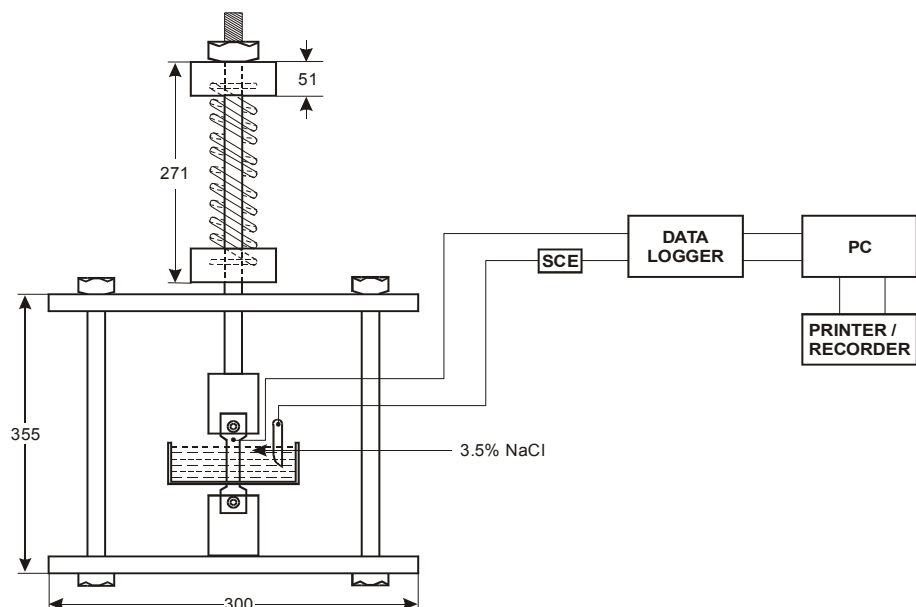


Figure 2: Spring loaded Tensometer

All dimensions are in mm

Electrochemical noise measurements were performed on flat specimen by using spring-loaded tensometer. The specimens were polished using successive grades of emery papers; 1/0, 2/0, 3/0 and 4/0 followed by fine polishing using buffing machine. The specimen was fixed in the plastic container and sealed by anabond-666 sealant. The corrosive medium, 3.5% NaCl solution, was used in stress corrosion testing. Saturated Calomel Electrode (SCE) was used as the reference electrode. The specimen acted as working electrode. No counter electrode was used. The corrosion potential was monitored by a 16 bit A/D (analogue/digital) data logger of 10 microvolt (μ V) least count and the overall accuracy, considering the noise from reference electrode, was 50 μ V. Electrochemical noise data was recorded after every one hour under different loading conditions; 50, 80 and 90% of yield stress,. The corrosion potential, (E_{corr}) values with time was recorded. The other parameters obtained from the corrosion potential vs. time were; E_{mean} (average E_{corr} value acquired by the sample during each set of measurement), $\Delta E_{initial}$ (difference between mean E_{corr} before application of the load and the E_{corr} value observed just after the application of the load), ΔE_{hyd} (Hydrogen evolution potential expressed as $E_{mean} - E_{HER}$, where E_{HER} is Nernst equilibrium potential for $H^+ / \frac{1}{2} H_2$ reaction at room temperature given by the relation 0 – 0.059 pH which works out to – 0.617 (SCE) and ΔE_{total} (difference between the final mean corrosion potential just before fracture and the mean potential just after the application of load). The Hurst exponent, H was calculated as quantitative parameter to compare signals. This exponent was evaluated using the Hurst rescaled range analysis [25]. Representative fractured surfaces from constant load test specimens were examined under scanning electron microscope (SEM) to identify the fracture modes.

Results and Discussion

Microstructure

Figure 3 (a-c) show typical microstructures for AA2219, AA8090 and AA5456 aluminium alloys. The variations in grain orientation can be observed from the microstructures. The grains were elongated in the rolling direction. The spherical precipitate particles were also seen in the microstructures. These precipitate particles have been reported [26] as $CuAl_3$, $CuMgAl_3$, $MgZn_2$, Al_2CuLi , $FeMnAl_6$, Mg_2Al_3 etc.

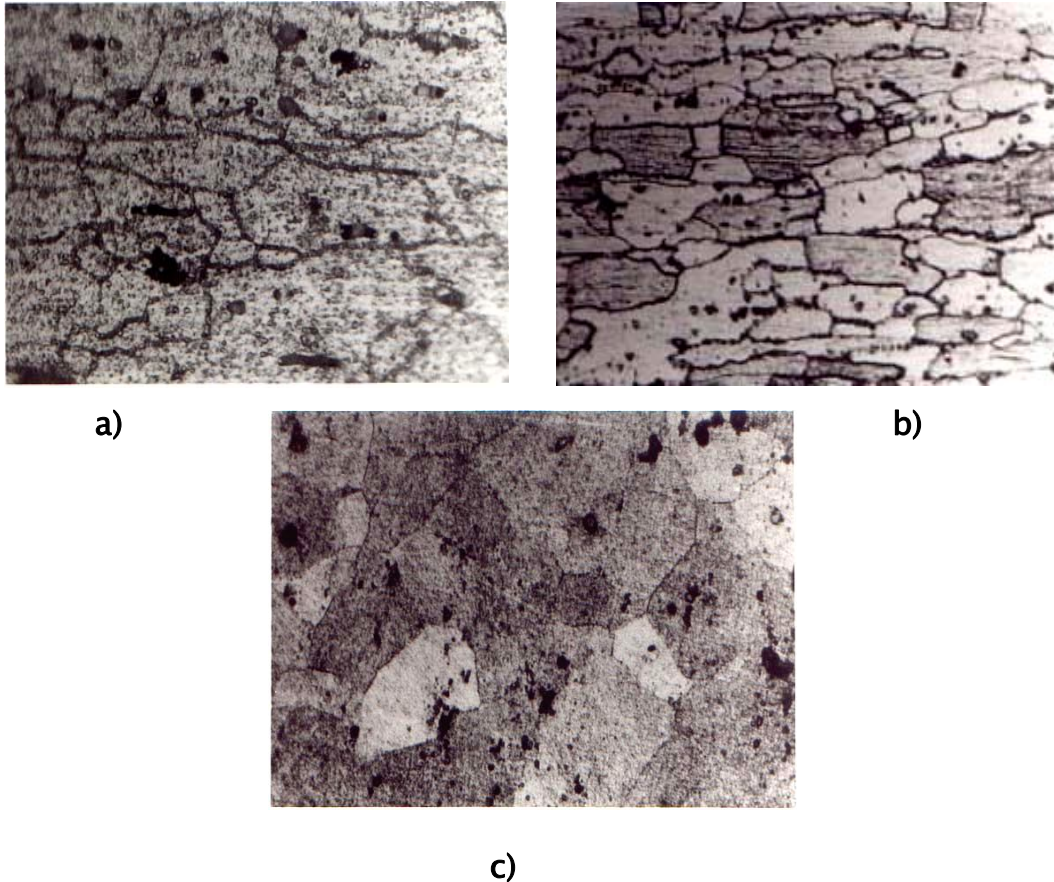


Figure 3: Microstructures of a) AA2219 b) AA8090 and c) AA5456 in long transverse directions at 100X.

Stress corrosion cracking studies

Figure 4–6 show corrosion potential vs. time noise pattern for AA 2219 alloy for peak aged and solution treated condition under the loading conditions of 50, 90 and 80 % of yield stress, respectively.

Figure 7–9 show corrosion potential vs. time noise pattern for AA 8090 alloy for peak aged and solution treated condition under the loading conditions of 50, 90 and 80 % of yield stress, respectively.

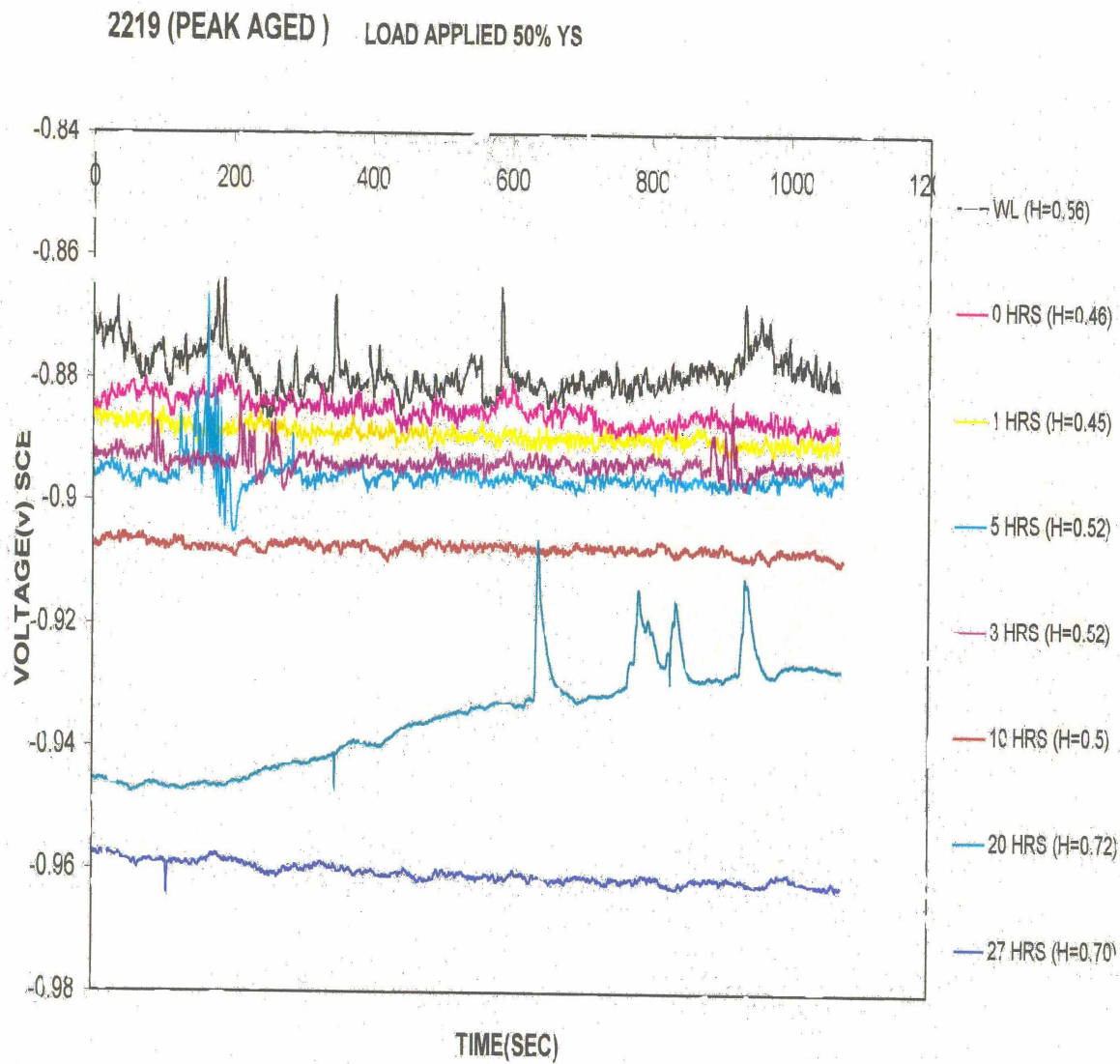


Figure 4: EN plots of AA2219 (peak aged) at 50 % YS load in 3.5 % NaCl solution.

2219(PEAK AGED) LOAD APPLIED 90%YS

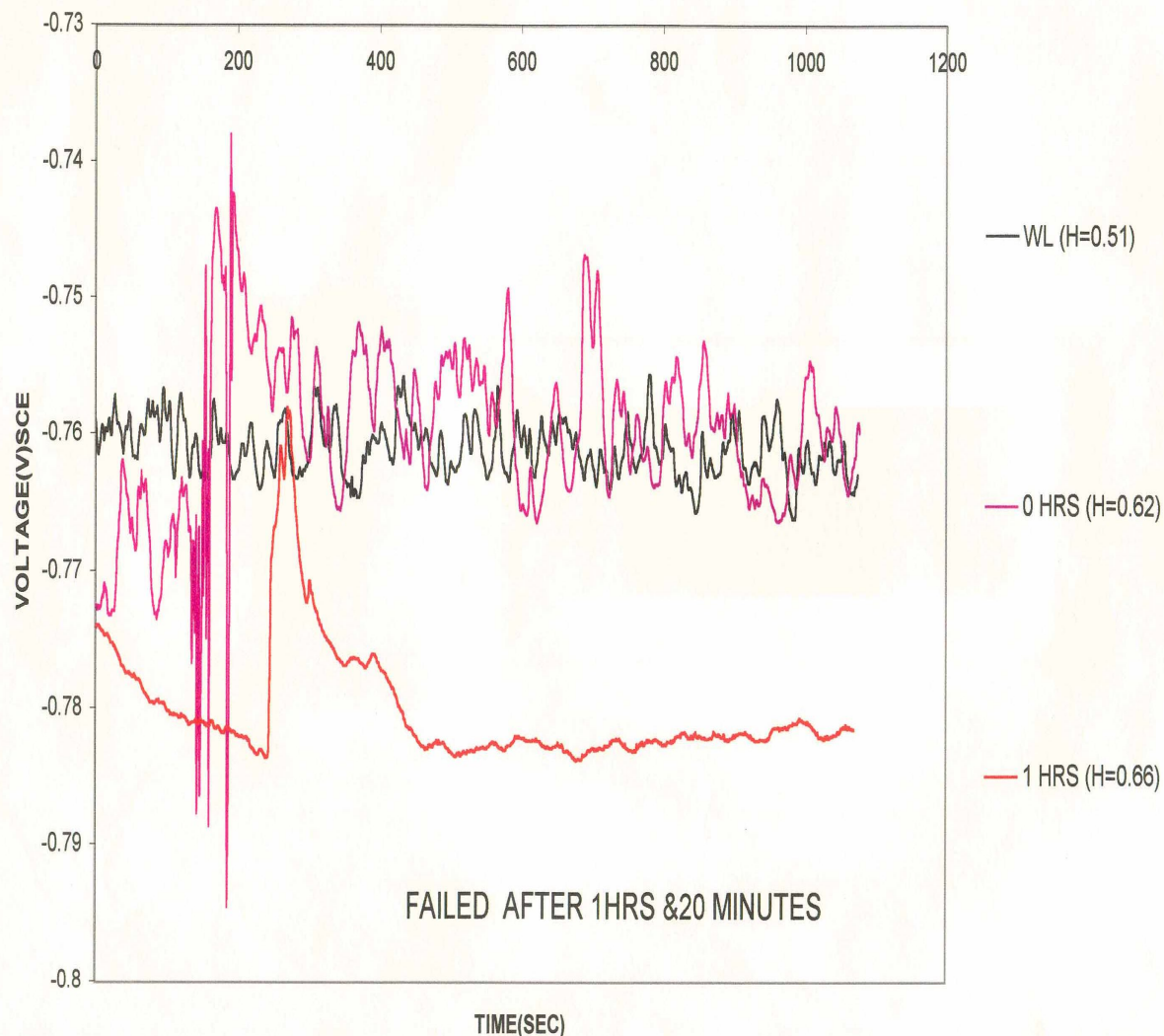


Figure 5: EN plots of AA2219 (peak aged) at 90 % YS load in 3.5 % NaCl solution.

2219(SOLUTION TREATED) LOAD APPLIED 80% YS

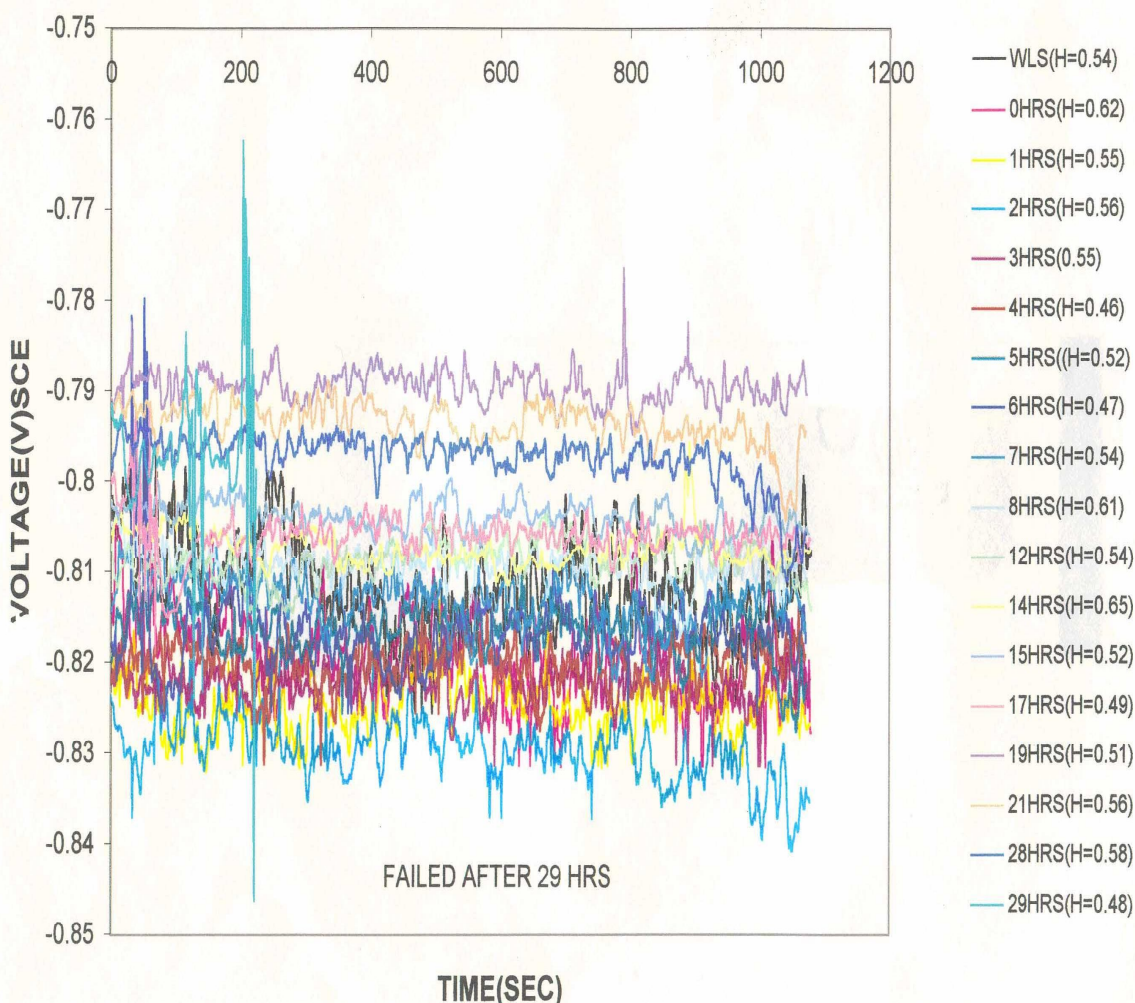


Figure 6: EN plots of AA2219 (solution annealed) at 80 % YS load in 3.5 % NaCl solution.

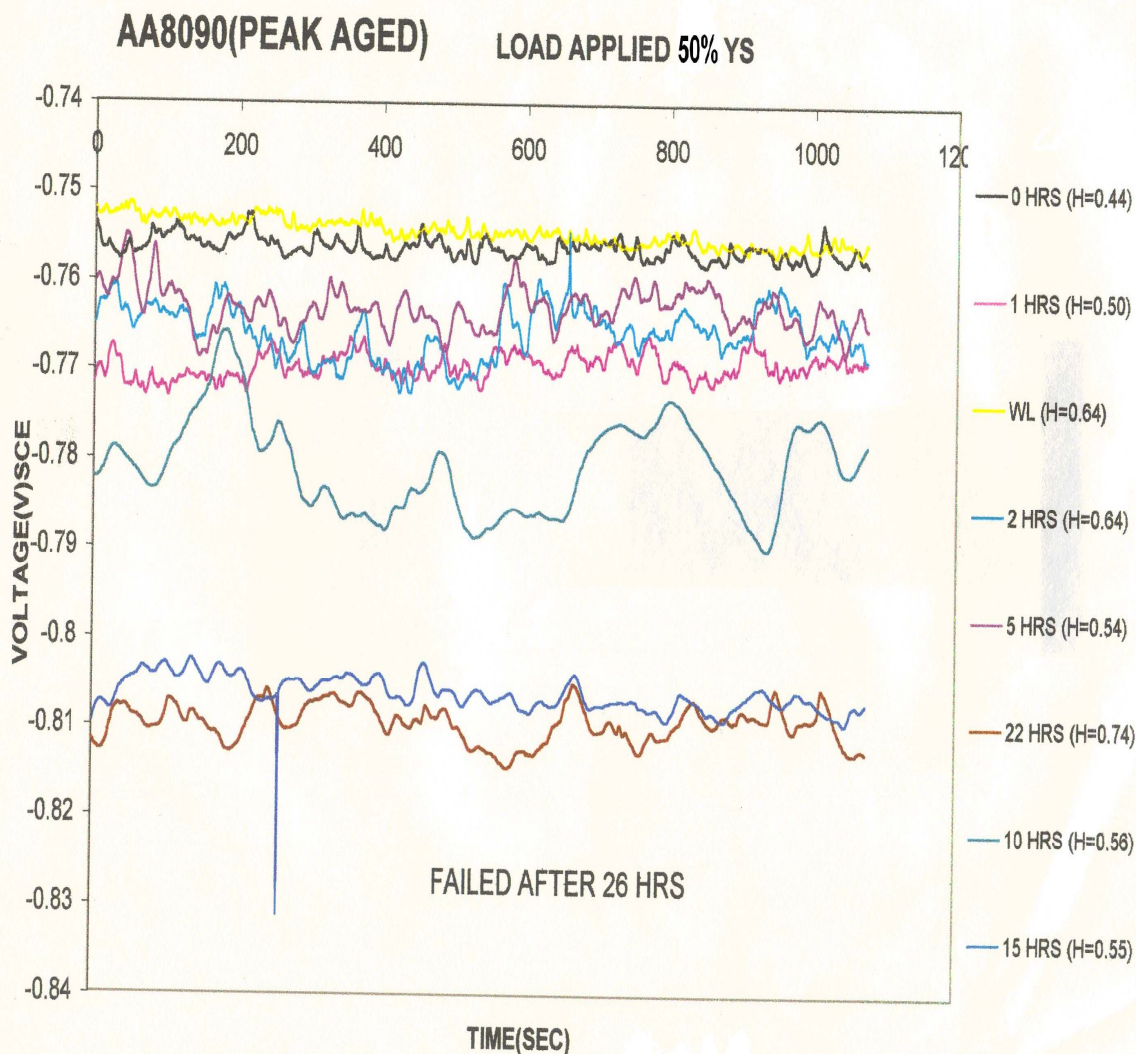


Figure 7: EN plots of AA8090 (peak aged) at 50 % YS load in 3.5 % NaCl solution.

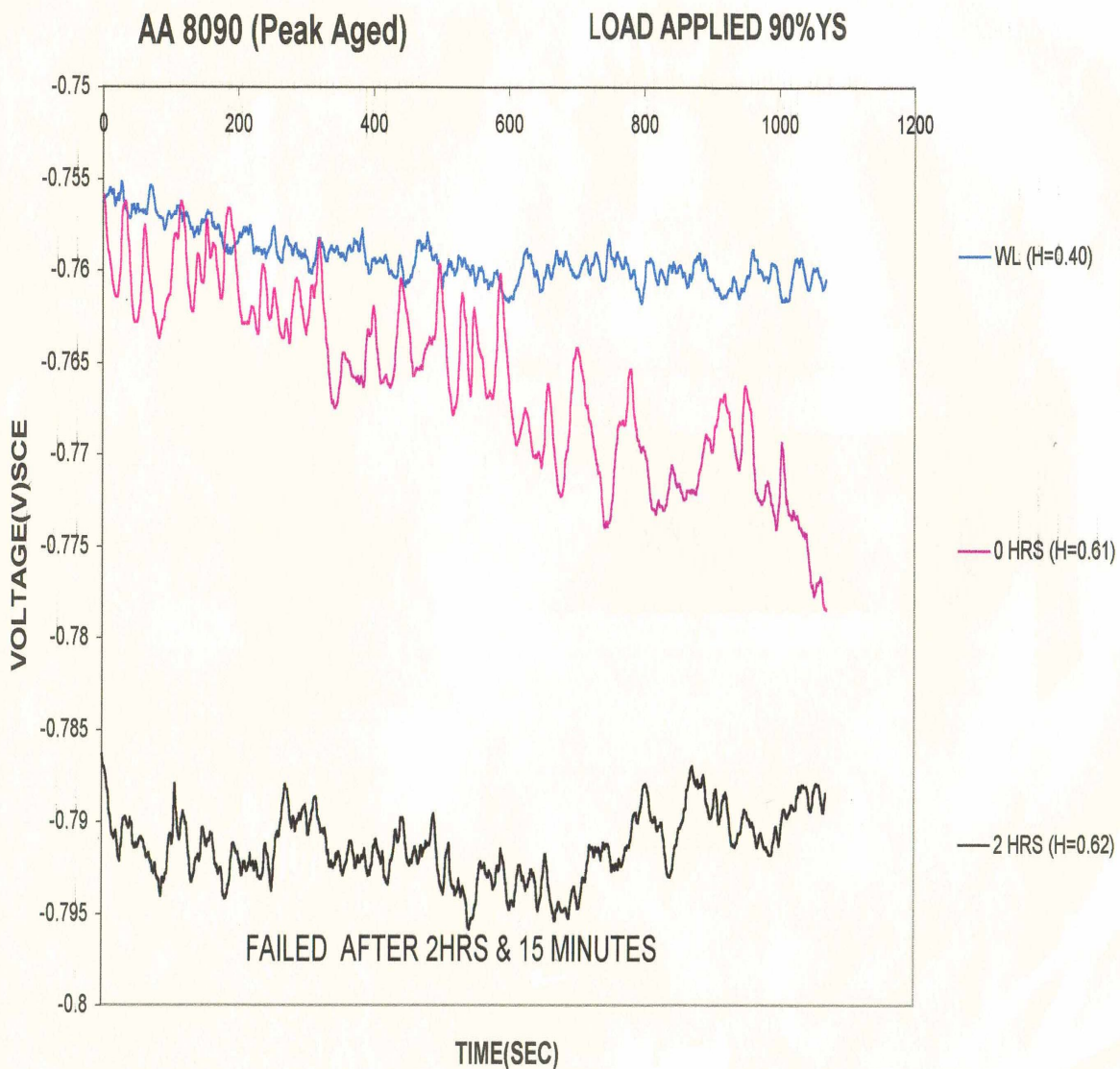


Figure 8: EN plots of AA8090 (peak aged) at 90 % YS load in 3.5 % NaCl solution.

8090(SOLUTION TREATED) LOAD APPLIED 80%YS

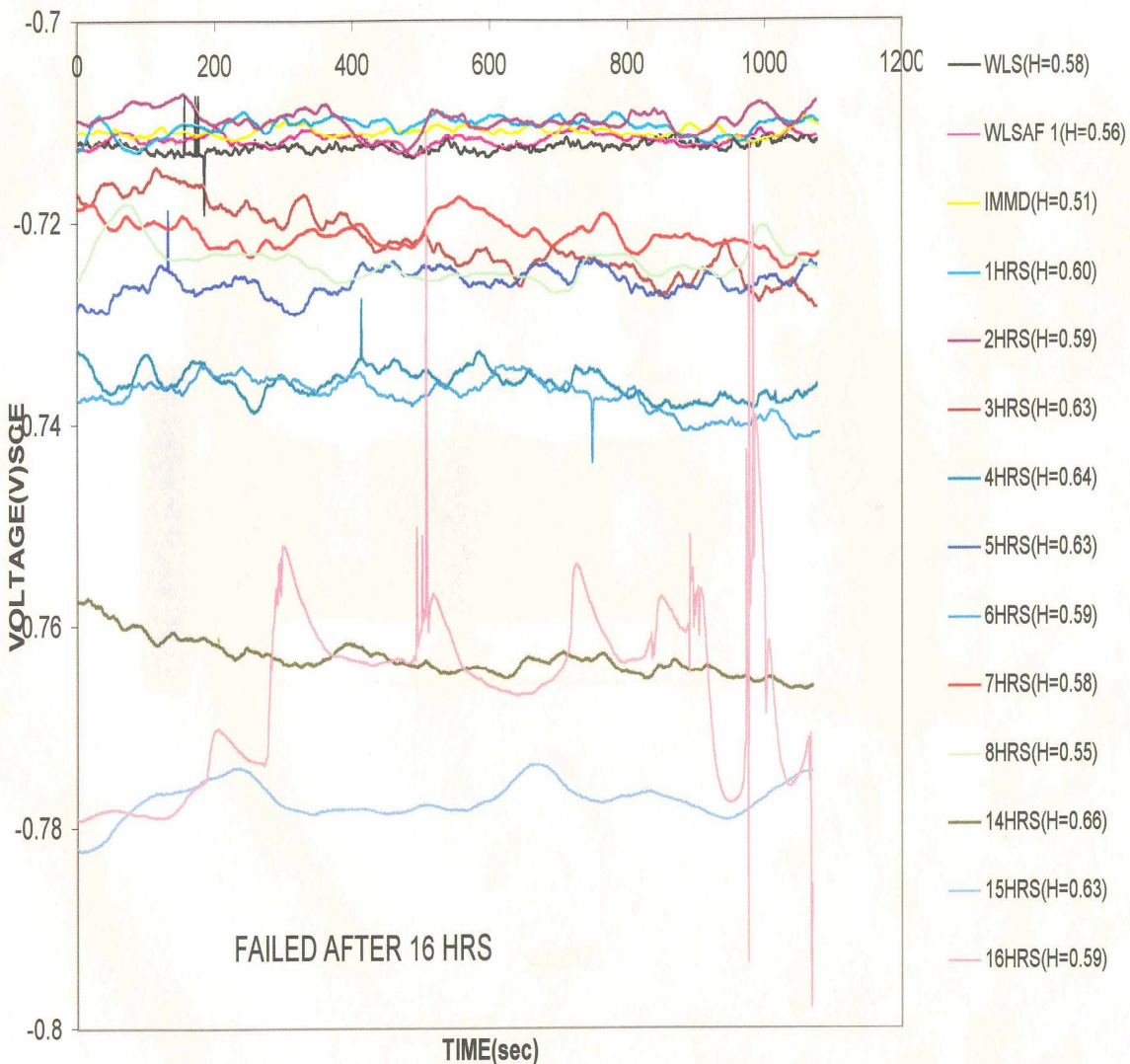


Figure 9: EN plots of AA8090 (solution annealed) at 80 % YS load in 3.5 % NaCl solution.

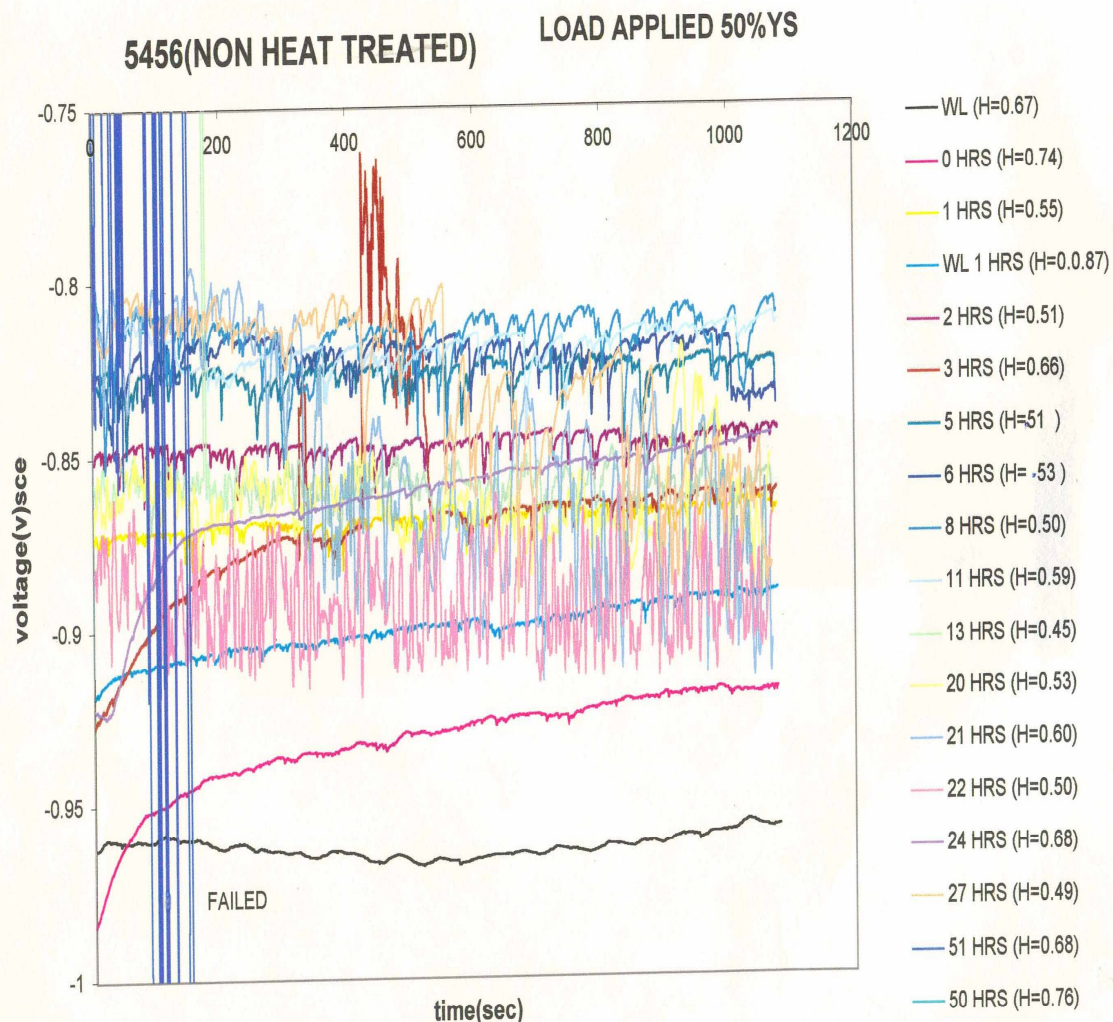


Figure 10: EN plots of AA5456 (strain hardened) at 50 % YS load in 3.5 % NaCl solution.

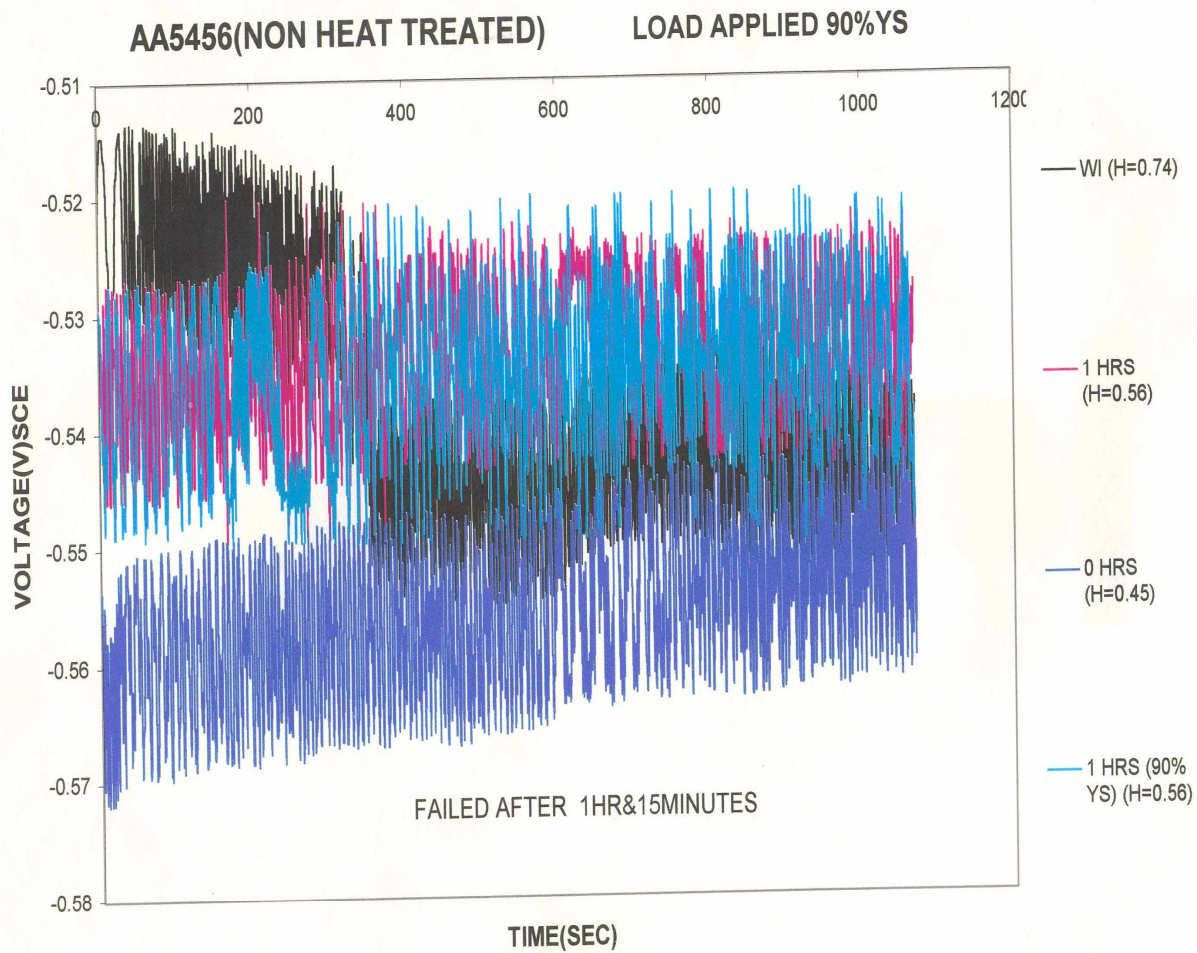


Figure 11: EN plot of AA5456 (strain hardened) at 90 % YS load in 3.5 % NaCl solution.

5456(SOLUTION TREATED) LOAD APPLIED 80%YS

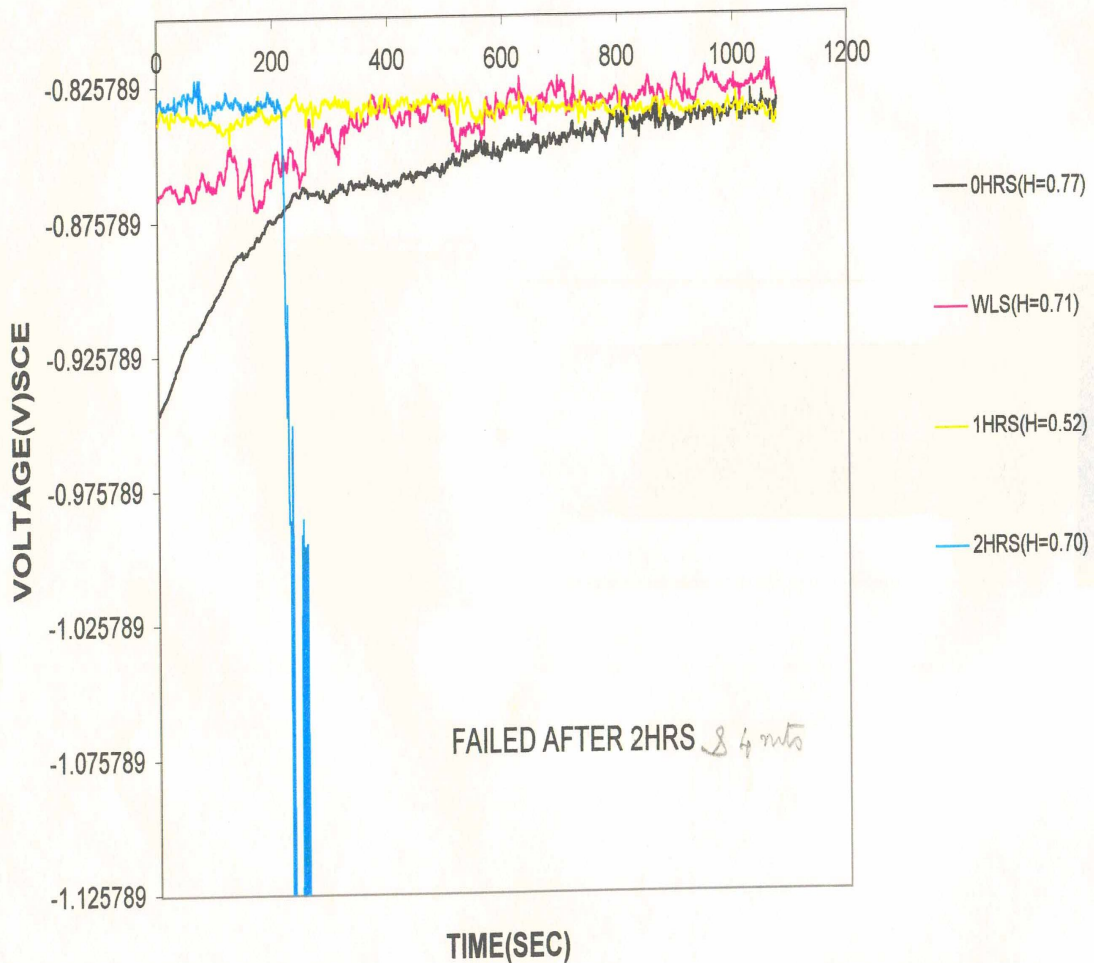


Figure 12: EN plots of AA5456 (solution annealed) at 80 % YS load in 3.5 % NaCl solution.

Figure 10–12 show corrosion potential vs. time noise pattern for AA 5456 alloy for strain hardened and solution treated condition under the loading conditions of 50, 90 and 80 % of yield stress, respectively.

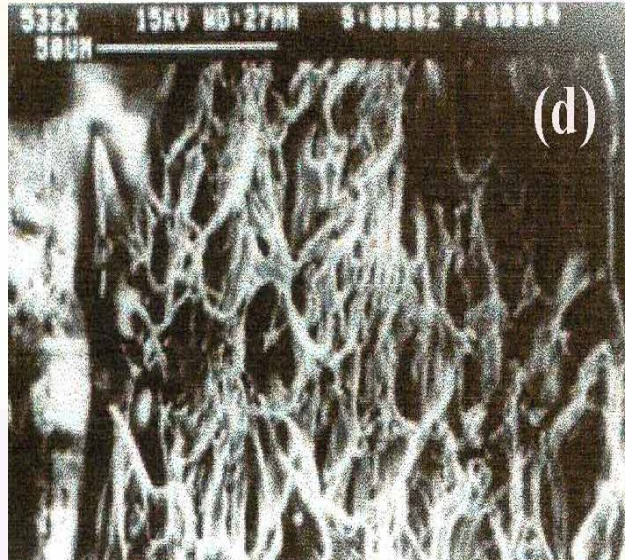
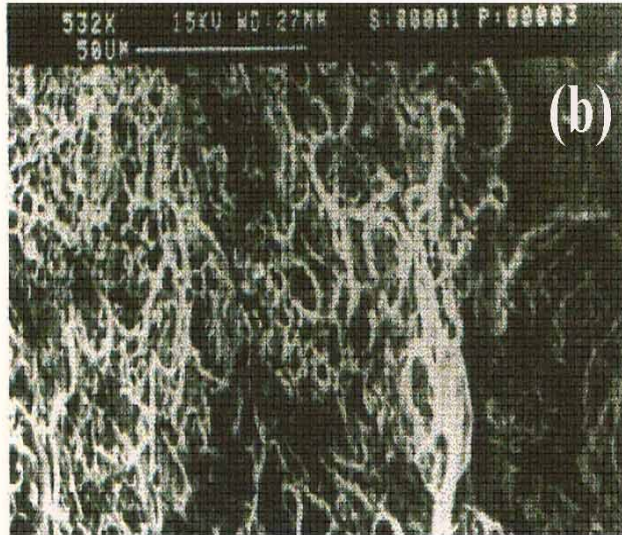
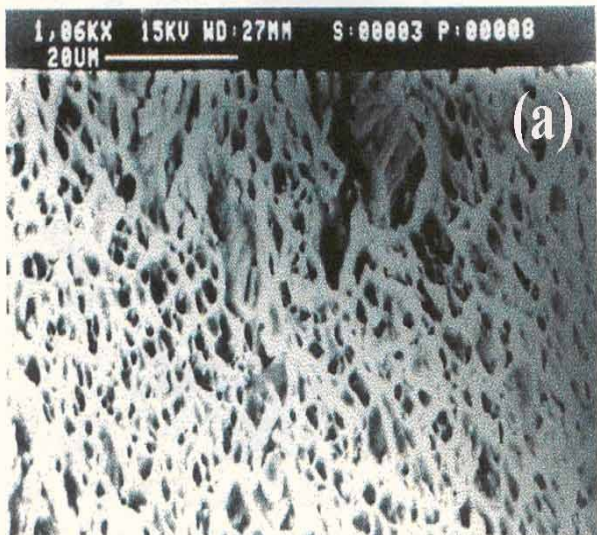


Figure 13: SEM photographs of SCC failed specimens: a) AA2219 (80% YS) b) AA8090 (load 80%YS) c) AA5456 (load 50% YS) and d) AA5456 (80%YS)

Figure 13 (a–b) shows SEM photographs of fractured surfaces after stress corrosion cracking tests for AA2219 and AA 8090 alloys under 80% yield stress loading conditions, respectively.

Figure 13 (c–d) shows SEM photographs of fractured surfaces of AA5456 and AA 5456 alloys under 50% and 80 % yield stress loading conditions, respectively.

It can be observed from figure 4–6 that in case of AA 2219 alloy, the specimen did not fail even after 27 hours when the load was 50 % of yield stress whereas the failure time was 1 hour and 20 minutes when the load applied was 90 % of yield stress, under peak aged condition. In comparison, solution treated specimen failed after 29 hours when the load was 80 % of yield stress. The corresponding time to failure was 26 hours 16 minutes and 2 hours 30 minutes under peak aged condition and 16 hours 20 minutes under solution treated condition for AA 8090 alloy with similar loading conditions as that of AA 2219 alloy as shown in figure 7–9. Under solution annealed condition in case of AA 5456 alloy failed after 51 hours when the applied load was 50 % of yield stress and 1 hour 30 minutes when the load was 90 % of yield stress under strain hardened conditions as shown in figure 10–12.

It can be observed that the noise pattern exhibited variation with time and significant changes were observed at the time of failure. The corresponding parameters $\Delta E_{\text{initial}}$, E_{mean} , ΔE_{hyd} and ΔE_{total} evaluated from the E_{corr} vs. time noise pattern were presented in table 3–6. It can be observed that there is drop in corrosion potential in case of 50%, 90% and 80% loading condition in case of AA2219 alloy. In both the cases; peak aged and solution annealed conditions, $\Delta E_{\text{initial}}$ is negative and is of the order of -15 mV as given in table 3. The drop in corrosion potential for AA 8090 alloys is less negative (-7 mV) as compared to that observed for AA 2219 alloy. Under solution annealed condition, the drop in corrosion potential was three times higher for AA 2219 alloy when compared to AA 8090 and AA 5456 alloys.

Table 4 gives ΔE_{total} values under different heat treatment conditions for AA2219, AA8090 and AA5456 alloys. It can be observed from table 4 that ΔE_{total} decreases as the magnitude of loading increases under peak aged condition for AA2219 and AA8090 alloys. Under solution annealed condition, ΔE_{total} value for AA 8090 alloy was two times more negative than that observed for AA 2219 alloy. In case of AA5456 alloy, ΔE_{total} values were positive under both, strain hardened and solution annealed condition.

Table 3 ΔE_{init} , initial corrosion potential immediately after application of loading.

Alloy	Temper	Load applied (% of YS)	Drop in corrosion potential ΔE_{init} (mV)
2219	Peak aged	50	-13
	Peak aged	90	-15
	Solution annealed	80	-15
5456	Strained hardened	50	-5
	Strain hardened	90	-22
	Solution annealed	80	-15
8090	Peak aged	50	-5
	Peak aged	90	-7
	Solution annealed	80	-5

Table 4 ΔE_{total} , total corrosion potential before fracture.

Alloy	Temper	Load applied (% of YS)	Total corrosion potential, ΔE_{total} (mV)
2219	Peak aged	50	-75
	Peak aged	90	-15
	Solution annealed	80	-25
5456	Strained hardened	50	80
	Strain hardened	90	25
	Solution annealed	80	25
8090	Peak aged	50	-55
	Peak aged	90	-20
	Solution annealed	80	-50

Table 5 Effect of load on average corrosion potential, E_{corr} and ΔE_{hyd}

Alloy	Load applied	E_{mean} (mV)	ΔE_{hyd} (mV)
2219	50	-0.885	-238
		-0.889	-242
		-0.895	-248

		-0.890	-243
		-0.91	-263
		-0.93	-283
		-0.96	-313
	90	-0.76	-113
		-0.815	-168
	80	-0.824	-177
		-0.825	-178
		-0.805	-158
		-0.819	-172
		-0.83	-183
5456		-0.87	223
	50	-0.85	203
		-0.97	323
		-0.88	233
	90	-0.535	112
		-0.94	293
	80	-0.83	183
		-0.828	184
8090		-0.753	-106
	50	-0.77	-123
		-0.755	-108
		-0.765	-118
		-0.762	-115
		-0.805	-150
		-0.814	-167
	90	-0.765	-118
		-0.79	-53
	80	-0.71	-63
		-0.715	-68
		-0.758	-111
		-0.078	-136
		-0.77	-123

Table 6 Fractographic features of corroded specimens as revealed by SEM observations.

Alloy	Load applied	Time to failure	Nature of fracture and morphological features
2219 Peak aged	90	1 hr and 38 minutes	Cracks gets elongated along rolling direction showing inter granular failure, Brittle failure
2219 Solution annealed	80	2 hrs and 20 minutes	Elongated dimples along the grain boundary indicating ductile failure
5456 Strain hardened	50	51 hrs	SCC failure due to crack opened along rolling direction.
5456 Strain hardened	90	1 hrs and 30 minutes	SCC failures due to crack gets elongated along grain boundary.
5456 Solution treated	80	2 hrs and 4 minutes	SCC failures, some ductile failure features also seen.
8090 Peak aged	50	26 hrs and 16 minutes	SCC failures due to crack elongated along rolling direction Brittle failure
8090 Peak aged	90	2 hrs and 30 minutes	SCC failures

Table 5 gives E_{mean} and ΔE_{hyd} values for AA2219, AA8090 and AA5456 alloys. It can be observed that ΔE_{hyd} values were relatively more negative in case of AA2219 alloy as compared to AA8090 alloy, irrespective of the magnitude of loading, whereas AA 5456 alloy exhibited positive ΔE_{hyd} values. ΔE_{hyd} values were of sufficiently negative for AA 2219 alloy in peak aged condition as compared to other aluminium alloys under 50 % yield stress loading conditions and no failure occurred even after 27 hrs. ΔE_{hyd} values in this case were

almost double as compared to 80% and 90% yield stress loading conditions which can be attributed to hydrogen-induced effect [27]. Higher values of ΔE_{hyd} were obtained due to hydrogen evolution during corrosion processes which is trapped at different microstructural sites; vacancies, dislocations, grain boundaries and precipitates and hydrogen also tends to get attracted to regions of high tri-axial tensile stress where the metal structure is dilated [28]. Therefore the dissolved hydrogen can cause fracture by assisting in the development of intense local plastic deformation [29]. It is suggested that loading condition is one of the important factors in deciding stress corrosion cracking resistance of AA 2219 alloy, which did not fail at 50 % yield stress loading condition and hydrogen induced effect could have led to its failure at higher level of loading condition. Under solution annealed and 80% yield stress loading condition, AA 8090 alloy exhibited significantly greater time for failure as compared to that of AA219 alloy. The ΔE_{hyd} and E_{mean} values were less negative in case of AA 8090 alloy as compared to AA 2219 alloy as given in table 6. The greater stress corrosion cracking resistance shown by AA 2219 under peak aged condition and AA 8090 alloy under solution annealed condition can be supported by SEM observations. Both these alloys showed mixed mode of failure as given in table 6 and shown in figure 13 (a-b). The ΔE_{total} and ΔE_{hyd} values of AA5456 alloy were different than the heat treatable alloy and became nobler with time suggesting re-passivation tendency leading to greater SCC resistance.

The morphological features of corroded specimens of AA5456 were presented in figure 13(c-d). The detailed description of nature of failure as seen from SEM micrographs was presented in table 6 and it can be observed that all the failures were highly brittle in nature and high values of ΔE_{hyd} seems to support the observation with time to failure decreased with increases in magnitude of loading.. Sharma et al [30] reported that the heat treatable alloys were inferior in corrosion resistance as compared to non heat treatable alloy due to formation of precipitates. In case of AA5456 alloy which was under non heat treated condition, absence of precipitate particles might have led to better corrosion resistance as indicated by nobler values of ΔE_{hyd} and greater time to failure as compared to other alloys. The Hurst exponent H was obtained by calculating slope of electrochemical potential time series data for all loading condition and the values of H were in the range of 0.45–0.72, 0.62–0.66 and 0.46– 0.65 in case of AA 22219 alloy under peak aged and solution treated conditions, respectively. The corresponding values of Hurst Exponents were 0.50–0.74, 0.62 and 0.51–0.66 for AA 8090 alloy whereas AA 5456 alloy exhibited H values in the range of 0.5–0.76, 0.56 and 0.52–0.70 under strain hardened and solution treated

conditions, respectively. The Hurst exponent values obtained from time series data showed variable tendency to be persistent as shown by E_{corr} vs. time plots, indicating constant change in surface activity of aluminium alloys. Higher values of H along with negative trends indicated that population of active sites was increasing leading to greater possibility of localized corrosion attack [25]. The similar results on Hurst exponent were reported by Sarmiento et al. [31] on corrosion inhibition of carbon steel and Gonzalez-Nunez et al. [19].

Conclusions

1. Corrosion potential vs. time noise patterns of heat treatable alloys (AA2219, AA8090) was different from non-heat treatable AA5456 alloy.
2. Electrochemical noise pattern exhibited variation with time and significant changes were observed at the time of failure.
3. The mean corrosion potentials were sufficiently negative to provoke hydrogen equilibrium reaction leading to hydrogen induced failure.
4. The magnitude of loading is one of the important factors in deciding stress corrosion cracking resistance of aluminum alloys.
5. The persistency of noise signals based on Hurst exponent varied with time. This signified constant change in the surface state of the material.

Acknowledgements

The authors acknowledge useful suggestions and comments by Dr. Rahul Khandagale, VIT Pune. Authors are thankful to Director, IIT Bombay for providing the necessary facilities for experimentation.

References

- [1] 'ASM Hanbook Committee, Aluminum and Aluminum alloys, Metals Handbook, ASM International' pp 3-159, 1993.
- [2] 'Corrosion of aluminum and aluminum alloys', J. G. Kaufman, *ASM International, Corrosion: Materials*, pp 95-124, 2005.

- [3] 'Localized corrosion of aluminum alloys- A Review', R. T. Foley, *NACE*, **42**, pp277–286, 1986.
- [4] 'Stress corrosion mechanisms for aluminum alloys', D. O. Sprol, R. H. Brown, *In International conference of fundamental aspects of stress-corrosion cracking, Houston: NACE International*, pp 469–512, 1969.
- [5] 'Fundamental of metallic corrosion', P. A. Schweitzer, *CRC Press, Taylor and Francis : 2nd ed*, pp 491–514, 2006 .
- [6] 'Interpretation of electrochemical noise data', R. A. Cottis, *Corrosion-NACE International* 2001, **57**, pp265–285, 2001.
- [7] 'Method of electrochemical noise measurement for characterization of local corrosion processes', J. Smulko, *Proceeding, World congress, Dubrovnik, Croatia 2003*.
- [8] 'Transient voltage changes produced in corroding metals and alloys', W. P. Iverson, *J. Electrochem society*, pp115:617, 1968.
- [9] 'Investgation of electrochemical processes by an electrochemical noise analysis: Theoretical and experimental aspect in potentiostatic regime', C. Gabrielli, F. Huet, M. Keddam, *Electrochimica Acta*, **31**, pp1025–1039, 1986.
- [10] 'Electrochemical noise measurement for corrosion applications', J. R. Kearns, *ASTM, Philadelphia*, 2002.
- [11] Electrochemical noise. Simulteneous monitoring of potential and current noise signals from corrding electrodes, DA. Eden, K. Hladky, D. G. John, J. L. Dawson, *paper 274 presented at "corrosion 91", NACE*, 1991.
- [12] 'Corrosion monitoring system based on measurement and analysis of electrochemical noise', A. Legal, V. Doleck, *Corrosion-NACE International*, **51**, pp295–300, 1995.
- [13] 'Long term storage in reservoirs: An experimental study,', H. E. Hurst, R. Black, Y. M. Sinaika, *Constable London*, 1965.

- [14] 'Range analysis of the corrosion potential noise', A. Horvath, R. Schiller, *Corrosion Science* 45 pp597–609, 2003.
- [15] 'Appliaction of Hurst exponent to the study of electrochemical noise signals', J. Sanchez-Amaya, F. Javier Botana, M. Bethencourt, *Corrosion, NACE International, New Orleans, La* 2004.
- [16] 'Noise analysis of pure aluminum under different pitting conditions', J. C. Urachurtu, J. L. Dawson, *Corrosion-NACE*, 43, pp 19–25, 1987.
- [17] 'Electrochemical noise as a possible method for detecting stress- corrosion- cracking', M. Leban, A. Legat, V. Dolecek, V. Kuhar, *Material science forum*, 289, pp157–162, 1998.
- [18] 'Electrochemical noise generation during stress corrosion cracking of high strength aluminum AA 7050-T6 alloy', C. A.Loto, R. A. Cottis, *Corrosion-NACE*, 45, pp137–141, 1989.
- [19] 'R/S Fractal analysis of electrochemical noise signals of three organic coating samples under corrosion conditions', M. A. Gonzalez-Nunez, J. Uruchurtu-Chavarin, *JCSE*, 6, pp1–15, 2003.
- [20] 'The influence of tensile stress on electrochemical noise from aluminum aloy in chloride media', X. F. Liu, J. Zhan, Q. J. Liu, *Corrosion Science*, 51, pp1460–1466, 2009.
- [21] 'Assessment of stress corrosion crack initiation and propogation in AISI type 316 stainless steel, by electrochemical noise technique', T. Anita, M. G. Pugar, H. Shaikh, R. K. Dayal, H. S. Khatak, *Corrosion Science*, 48, pp2689–2710, 2006.
- [22] 'Comparision of susceptibility to pitting corrosion of AA 2024-T4, AA7075-T651 and AA7475-T761 aluminum alloys in neutral chloride solutions using elecrochemical noise analysis', K. Na, Su – II Pyun, *Corrosion Science*, 50, pp248–258, 2008.
- [23] 'Stress corrosion cracking test method', A. J. Sedrik, *National Association of Corrosion Engineer*, pp1–18, 1991.

[24] 'Design of machine elements', M. F. Spotts, 6th ed., *Prentice Hall, Englewood Cliffs, New Jersey* 1985.

[25] 'Rescaled range analysis of random events', F. Pallikari, E.A. Boller, *Journal of scientific exploration*, 13, pp25–40, 1999.

[26] 'Metallographic techniques and Microstructures', *ASM Hanbook Committee, Aluminum alloys, ASM International*, 1992.

[27] 'The influence of hydrogen on the stress-corroson cracking of low-strength Al-Mg alloy', R.H. Jones, J. JOM Miner, *Met. Mater. Soc.*, 55, pp42–46, 2003.

[28] 'Corrosion-induced hydrogen embrittlement in aluminum alloy 2024', H. Kamoutsi, G. N. Haidemenopoulos, V. Bontozoglou, S. Pantelakis, *Corrosion Science*, 48, pp1209–1224, 2006.

[29] 'Evidence on the corrosion-induced hydrogen embrittlement of the 2024 aluminum alloy', P.V. Petroyiannis, E. Kamoutsi, A. T. Kermanidis, S. G. Pantelakis, V. Bontozoglou, G. N. Haidemenopoulos, *Fatigue Fract. Engg. Mater Struct.*, 28, pp565–574, 2005.

[30] 'Engineering Materials: Properties and Application of Metals and Alloys', C.P. Sharma, *Prentice-Hall of India, New Delhi*, 2005.

[31] 'Fractal ananlysis of the corrosion inhibition of carbon steel ina bromide solution by lithium chromate', E. Sarmiento, J. G. Gonzalez-Rodriguez, J. Uruchurtu, J. Sarmiento, M. Menchaca, *Int. J. Electrochem sci.* 4, pp144–155, 2009.